Physica Medica 76 (2020) 285–293

Contents lists available at ScienceDirect

Physica Medica

journal homepage: www.elsevier.com/locate/ejmp

Technical note

Personalized treatment planning in eye brachytherapy for ocular melanoma: Dosimetric analysis on ophthalmic structure at risk

F. Itta[a], R. Liuzzi[b], A. Farella[c], G. Porri[c], R. Pacelli[c], M. Conson[c], C. Oliviero[d], F. Buonanno[a], M.A. Breve[e], G. Cennamo[f], S. Clemente[d,1], L. Cella[b,*,1]

[a] University Federico II, Post Graduate School in Medical Physics, Department of Advanced Biomedical Sciences, Napoli, Italy
[b] National Research Council (CNR), Institute of Biostructures and Bioimaging, Napoli, Italy
[c] University Federico II, Department of Advanced Biomedical Sciences, Napoli, Italy
[d] University Hospital Federico II, Unit of Medical Physics and Radioprotection, Napoli, Italy
[e] University Federico II, Department of Neurosciences, Reproductive Sciences and Dentistry, Napoli, Italy
[f] University Federico II, Eye Clinic Department of Public Health, Napoli, Italy

ARTICLE INFO

Keywords:
Ru-106
Eye plaque brachytherapy
Ocular melanoma
CT-based eye-model
Ophthalmic structures-at-risk
Personalized treatment planning

ABSTRACT

Purpose: To evaluate the impact on dose distribution to eye organs-at-risk (eOARs) of a computed tomography (CT)-based treatment planning in eye plaque brachytherapy (EPB) treatment.
Methods: We analyzed 19 ocular melanoma patients treated with ruthenium-106 plaques to a total dose of 100 Gy to tumor apex using conventional central-axis-point dose calculation. Treatments were re-planned using the Plaque Simulator (PS) software implementing two different strategies: a personalized CT-eye-model (CT-PS) and a standard-eye-model (SEM-PS) defined by Collaborative Ocular Melanoma Study. Dice coefficient and Hausdorff distance evaluated the concordance between eye-bulb-models. Mean doses (D_{mean}) to tumor and eOARs were extracted from Dose-Volume-Histograms and Retinal-Dose-Area-Histogram. Differences between planning approaches were tested by Wilcoxon signed-rank test.
Results: In the analyzed cohort, 8 patients (42%) had posterior tumor location, 8 (42%) anterior, and 3 (16%) equatorial. The SEM did not accurately described the real CT eye-bulb geometry (median Hausdorff distance 0.8 mm, range: (0.4–1.3) mm). Significant differences in fovea and macula D_{mean} values were found ($p = 0.04$) between CT-PS and SEM-PS schemes. No significant dosimetric differences were found for tumor and other eOARs. The planning scheme particularly affects the OARs closest to the tumor with a general tendency of SEM-PS to overestimate the doses to the OARs closest to the tumor.
Conclusion: The dosimetric accuracy achievable with CT-PS EPB treatment planning may help to identify ocular melanoma patients who could benefit the most from a personalized eye dosimetry for an optimal outcome in terms of tumor coverage and eOARs sparing. Further research and larger studies are underway.

1. Introduction

Ocular melanomas are the second most common type of melanoma after the cutaneous form and the most common primary ocular malignancies with an incidence of two cases per million in Southern Europe [1]. Ocular melanomas typically appear as dome shaped mounds rising from the sclera shell of the eye. Currently, depending on tumor position and dimension several treatment options exist such as enucleation, charged particle irradiation, stereotactic photon radiotherapy and eye plaque brachytherapy (EPB) [2]. Enucleation has been the standard treatment for all type of ocular melanomas until the 80's [2]. A large trial, the Collaborative Ocular Melanoma Study (COMS), demonstrated no differences in survival between patients treated with EPB vs enucleation [3]. Today EPB represents the standard treatment modality for small and medium sized ocular tumors, iso-effective to proton therapy [2], as it combines eye preservation with tumor growth control. The most common radioisotopes used in EPB treatments are the gamma emitter iodine-125 (I-125) and the beta emitter ruthenium-106 (Ru-106). I-125 plaques are fabricated using multiple seeds imbedded in a concave gold plaque while in Ru-106 plaques the isotope is almost equally distributed on the concave surface of a shell shaped applicator.

The use of Ru-106 eye plaques has been the treatment of choice for

* Corresponding author at: National Research Council, Institute of Biostructures and Bioimaging, Via T. De Amicis, 95, 80145 Napoli, Italy.
E-mail address: laura.cella@cnr.it (L. Cella).
[1] These authors share the senior authorship.

https://doi.org/10.1016/j.ejmp.2020.07.019
Received 21 May 2020; Received in revised form 14 July 2020; Accepted 15 July 2020
Available online 29 July 2020

small to medium sized ocular melanomas (maximum thickness less than 6.5 mm) thanks to a very steep dose fall-off within few millimeters from the surface of the applicators [4–7]. Furthermore, Ru-106 plaques allow simple radioprotection procedures compared to I-125 seeds loaded plaques [8,9] and also better toxicity profiles for critical ophthalmic structures at risk such as the retina, macula, fovea, optic disc and lens [8].

In the conventional Ru-106 EPB workflow, tumor dimension (apex height and basal diameters) and its location on the retinal chart are defined by using ophthalmic scan ultrasound (US) and ocular fundus images [10]. The ophthalmic applicator that best fits the tumor basal dimension is selected amongst various diameters (15–23 mm) and shapes. The selected Ru-106 plaque applicator is then surgically placed beneath the tumor base by the ophthalmologist and its eyelets sutured to the sclera to affix its position for the time necessary to deliver the tumor prescription dose. Different dose prescriptions for the tumor are suggested, with apical doses ranging from 60 to 130 Gy [5,8,10]. The estimation of implant duration time (typically 2–7 days) is generally based on plaque central-axis-point dose rate data coming from the plaque calibration datasheet provided by the manufacturer. Although, this conventional approach guarantees the coverage of the tumor with the prescribed dose, it does not provide any quantitative evaluation of the doses received by the eye organs-at-risk (eOARs) due to the lack of an image-based dose map calculation involving the ocular anatomy, which is treated as a homogeneous water sphere [11,12]. The accuracy of treatment doses is however crucial given the small size of the eye structures and the steep dose gradients produced by EPB applicators.

In this framework, a three-dimensional (3D) patient specific image-guided treatment planning approach would guarantee an optimal treatment outcome in terms of both tumor control and eOARs sparing so as to avoid radiation induced complications (cataract, maculopathy, neuropathy, retinopathy) [13] that still remain an issue for most EPB patients.

Today very few image-based treatment-planning systems for ocular brachytherapy exist such as some in-house software solutions [14–16] and there is only one commercially available solution, the Plaque Simulator (PS, v6.6.6. Eye Physics LLC, Los Alamitos, CA) software [17], although not certified for the clinical use [18]. PS is a 3D treatment simulation and modeling package for EPB of ocular tumors. This software allows creating patient specific 3D eye and tumor models by using fundus images, US and either Computed Tomography (CT) or Magnetic Resonance (MR) images. However, CT or MR imaging are not always available in the clinical EPB practice. In these cases, a standard eye-model (SEM) defined by COMS [19] could be used for planning in PS.

In the present study, we evaluated the dosimetric impact on eOARs of the introduction of CT-based treatment planning in Ru-106 EPB using PS software. In addition, a dosimetric comparison between a patient specific eye geometry planning (CT-PS) vs. a standard eye geometry-based planning (SEM-PS) was performed.

The evaluation of the potential gain achievable with CT based EPB treatment planning may be useful for identifying those patients who could take maximum advantage from a personalized eye dosimetry in EPB with the aim of ensuring the optimal treatment outcome in terms of tumor coverage and eOARs sparing.

2. Materials and methods

2.1. Patients

For the present in silico study, we examined 19 ocular melanoma patients treated with EPB at University Federico II of Naples from March 2019 to February 2020. Patient's and tumor characteristics were reported in Table 1. Patients were classified according to their tumor position on the retinal chart (Fig. 1A) as follows:

- A (Anterior): Tumor center position behind the retinal chart ora line;

Table 1
Summary of patients' data, tumor and treatment characteristics.

Patient	Sex	Age	Pathology	Eye	Tumor location	Clock position (a.m.)	Tumor Apex height (mm)	Tumor Basal diameters		1D implant duration (h)	PS implant duration (h)
								Long (mm)	Lat (mm)		
#pt1	F	55	Choroidal melanoma	L	A	2:30	2.8	10.0	6.0	32.8	33.5
#pt2	F	46	Iris melanoma	R	A	1:30	6.5	6.8	5.0	126.5	121.4
#pt3	M	75	Choroidal melanoma	L	A	2:30	4.0	8.0	4.0	42.3	42.8
#pt4	M	43	Iris melanoma	R	A	7:30	3.0	5.0	5.0	38.0	39.0
#pt5	M	47	Choroidal melanoma	L	A	2:00	3.5	7.0	5.0	36.7	34.9
#pt6	M	46	Iris melanoma	R	A	9:00	3.0	5.0	5.0	35.6	36.4
#pt7	M	71	Choroidal melanoma	R	A	6:30	3.0	5.5	5.0	45.0	46.5
#pt8	F	84	Choroidal melanoma	L	A	11:00	6.5	5.0	6.0	151.8	148.3
#pt9	F	71	Choroidal melanoma	L	E	3:30	2.8	7.8	5.8	36.3	34.9
#pt10	F	79	Choroidal melanoma	L	E	3:00	3.2	9.7	5.4	35.9	35.8
#pt11	M	79	Choroidal melanoma	L	E	10:00	3.5	5.3	5.0	45.2	46.2
#pt12	F	73	Choroidal melanoma	R	P	4:00	3.2	6.5	13.7	27.2	25.4
#pt13	M	70	Choroidal melanoma	R	P	6:30	4.0	6.5	9.0	38.6	39.2
#pt14	M	61	Choroidal melanoma	R	P	8:00	3.0	10.0	4.0	29.0	29.5
#pt15	M	60	Choroidal melanoma	R	P	10:00	6.0	6.0	11.5	65.9	67.8
#pt16	M	68	Choroidal melanoma	L	P	4:00	3.0	6.0	10.6	26.1	26.5
#pt17	M	32	Choroidal melanoma	L	P	3:30	6.5	11.6	7.0	101.5	97.0
#pt18	F	62	Choroidal melanoma	L	P	6:00	3.3	4.0	8.5	34.4	34.9
#pt19	F	74	Choroidal melanoma	R	P	7:30	3.0	6.5	6.0	44.5	45.6

Abbreviations. pt: patient, A: anterior, E: equatorial, P: Posterior, R: right, L: Left, F: female, M: Male, am: anti meridian, Long: Longitudinal, Lat: latitudinal.

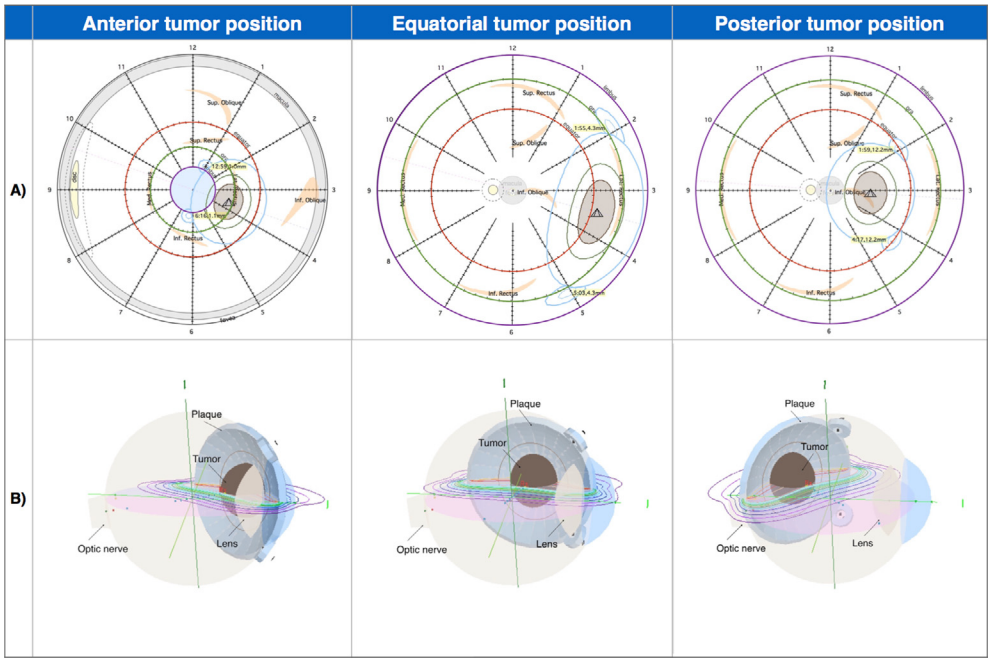

Fig. 1. a) Anterior, Equatorial, Posterior tumor (brown shape) and plaque (blu line) position on the retinal chart (RC): and b) the corresponding 3D model.

- E (Equatorial): Tumor center position between the retinal chart equator and ora lines;
- P (Posterior): Tumor center position beyond the retinal chart equator line.

All patients were treated with Ru-106 EPB to a total dose of 100 Gy to the tumor apex. According to the conventional central-axis-point dose calculation (1 D treatment planning) [6], the time of implant duration, T, for a tumor height z (prescription depth) was:

$$T = \frac{D}{\dot{D}_{\mathrm{corr}}(z)} \tag{1}$$

where D was the prescription dose, $\dot{D}_{\mathrm{corr}}(z)$ was the dose rate at the depth z at the time of plaque insertion (t) given by

$$\dot{D}_{\mathrm{corr}}(z) = \dot{D}_0(z) \cdot e^{(t-t_0)\cdot \frac{\ln 2}{T_{1/2}}} \tag{2}$$

where $\dot{D}_0(z)$ is the dose rate at the depth z at plaque calibration time (t_0) and $T_{1/2}$ the radionuclide half-life.

In Table 1, for each patient, tumor characteristics (apex height and basal diameters) obtained from US and confirmed by CT images, and implant time durations were reported.

2.2. Eye plaques

Ru-106 ophthalmic plaques CCB type (Eckert & Ziegler BEBIG, Berlin, Germany) were used. CCB Ru-106 applicators are spherically concave silver bowl with a diameter of 20 mm. The total shell thickness of 1 mm and it is divided into three layers of thickness, from the inner to outer, of 0.1, 0.2 and 0.7 mm. All layers are made of silver with the middle layer containing the emitter substance. The radioactive nuclide is electrically deposited with an approximate thickness of 0.1 μm on the concave surface [20].

The Ru-106 (half-life 374 days) disintegrates via β-decay with a peak beta particle energy of 39 KeV to the radioactive daughter Rh-106. The primary contributor to therapeutic dose is the continuous spectrum of beta particles emitted in the decay of Rh-106 (half-life 30 s). Rh-106 disintegrates by β- decay with a mean beta energy of about 1.4 MeV and a maximum of 3.5 MeV to the stable element Pd-106.

The 90-percentile distance for Rh-106 beta particles in water is 7.9 mm. Backscatter from the 0.7 mm thick silver backing of the applicator tends to soften the spectrum [21].

2.3. EPB planning

All patients were re-planned on purpose by the PS software using two different planning schemes. The first strategy was based on a personalized CT eye-model geometry. For each patient, head CT scans were acquired (Internal Review Board protocol, n. 222–10) at Toshiba Aquilion Multi, 4 Slice CT scanner. CT images were acquired by setting scan parameters able to provide acceptable CT image quality required for patient specific eye and tumor models (200 mA, 120 kVp, 0.5 mm slice thickness, 512 × 512 pixels). The second planning scheme was based on the SEM geometry with a standard eye equatorial diameter of 24 mm, as established by COMS. The whole pipeline is illustrated in Fig. 2.

As an ancillary analysis, the implant duration time estimated by the PS software was verified against the implant duration time of the actual treatment obtained with the 1D planning calculation.

2.4. Eye modeling: CT-PS scheme

First, the acquired CT data set was imported in Horos software Version 3.3 (Nimble Co LLC d/b/a Purview in Annapolis, MD USA) for multiplanar reconstruction. Axial, equatorial and sagittal 2D eye cross sectional images (2D-CSI) were then generated for eye modelling. Similarly, in Horos software, tumor coronal and meridian 2D-CSI were extracted for tumor modelling. For each patient, an expert radiation oncologist (G.P.) manually segmented on the CT-the eyeballs, lens and optic nerve. A dedicated tool available in the PS software was used to fit the segmented structures and tumor on the 2D-CSI. Finally, the software automatically generated the patient specific best-fitted 3D eye-model including retina, fovea, and macula structures [22]. For each 3D model, the following eye parameters, as defined by COMS [19], were extracted:

- Equatorial diameter: length of the eyeball equatorial diameter;
- Anterior-posterior (AP) axis: length of the eyeball AP axis (perpendicular to the equatorial diameter);
- Limbus diameter: diameter of the limbus circumference;

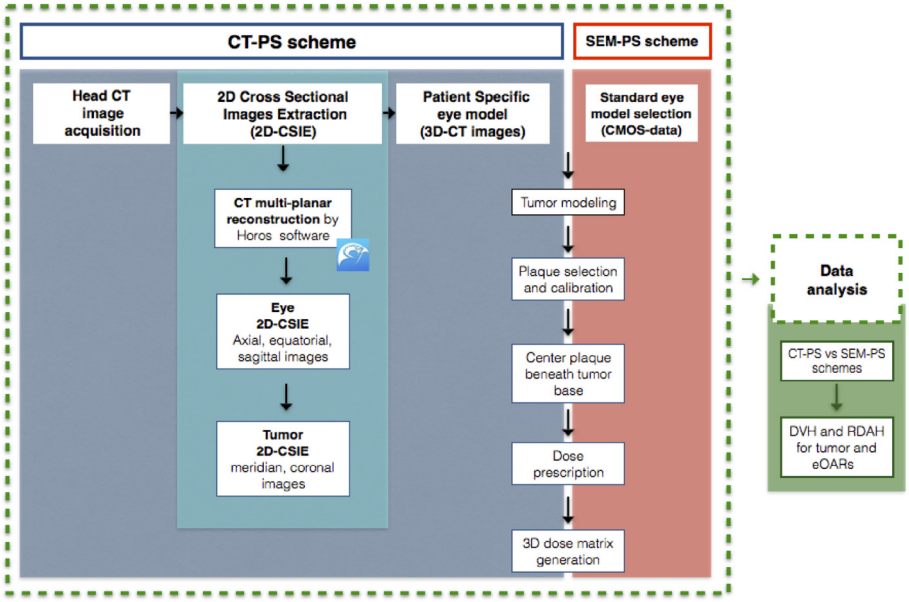

Fig. 2. Workflow of planning strategies implemented.

- Lens diameter: diameter of the lens circumference;
- Disc to pole angle: angle between the optic nerve and the eye AP axis;
- Disc to pole chord length: length of the chord beneath the disc to pole angle;

2.5. Eye modeling: SEM-PS scheme

For each patient, the 24 mm eye equatorial diameter was implemented in the PS software with the following COMS eye parameters' set: AP axis = 26.2 mm, Limbus diameter = 12 mm, Lens size = 10 mm, Disc to pole angle = 21.9 deg, Disc to chord length = 4.2 mm. For each patient, the treatment planning was repeated by using the PS software with the SEM geometry.

Once completed the eye and tumor-modeling steps via CT-PS and SEM-PS schemes, in order to reproduce the tumor center position on the RC, the optic disc to tumor center (OD-TC) distance, obtained from US and CT clinical images, was used as reference.

Then, the CCB Ru-106 eye plaque was calibrated in the PS software, using the patch source model approach [20]. The plaque was then virtually centered beneath the tumor base for each patient. The prescribed dose of 100 Gy to the tumor apex was set and a 3D dose matrix was automatically generated.

2.6. Data analysis: 3D eye geometry and dosimetric evaluation

The concordance between CT and SEM eye-bulb models was evaluated in terms of Dice coefficient [23] and of Hausdorff distance [24] by using a mesh-based approach within the 3D Slicer environment [22]. The Dice coefficient and Hausdorff distance are commonly used spatial similarity metrics for evaluating 3D medical image segmentation [25].

The volumes of CT and SEM eye-bulbs were compared by Dice coefficient. Given two sets of segmentations a and B, the Dice coefficient is given by

$$\mathrm{Dice}(A, B) = 2 \bullet \frac{|A \cap B|}{|A| + |B|} \tag{3}$$

A Dice score of zero indicates no overlap, whereas a score of one indicates full overlap.

The surfaces of CT and SEM eye-bulbs were compared by the Hausdorff distance. Let M be a metric space and $\varnothing \neq A,B \subset M$ compact subsets, the Hausdorff distance is defined as

$$h(A,B)=\max\{\mathrm{dist}(A,B), \mathrm{dist}(B,A)\} \tag{4}$$

Where

$$\mathrm{dist}(A, B) = \sup_{x \in A} \inf_{y \in B} d(x, y) \tag{5}$$

The lower the Hausdorff distance value, the closest is the matching.

Dose-Volume-Histograms (DVHs) were computed for the tumor volume and for lens, while retinal dose area histogram (RDAH) [26] were computed for the retina, tumor base, macula, fovea and the optic disc. The mean dose (D_{mean}) for each structure was then extracted.

For each patient, the D_{mean} to the macula and D_{mean} to the optic disc, as a function of the OD-TC distance, were also evaluated.

Dosimetric differences between the two planning approaches, CT-PS and SEM-PS, were analyzed. The median value and their range were employed to describe all continuous variables, and the non-parametric Wilcoxon matched-pairs signed-rank test was used to determine statistically significant differences between groups. Statistical analyses were performed using SPSS software, version 16.0 (SPSS Inc, Chicago, IL, USA) taking p less than 0.05 as statistically significant.

3. Results

3.1. Implant time duration

In the analyzed cohort, median plaque implant time duration calculated by the PS software (Table 1) was 39.0 hs (range [25.4–148.3] hs) compared with 38.0 hs (range [26.1–151.8] hs) calculated according to Eq. (1). The difference was not statistically significant (p = 0.97).

3.2. Tumor and eye-bulb 3D modelling

Ten out of 19 (53%) patients were diagnosed with tumor on the left eye and 9 out of 19 (47%) patients on the right eye. Tumor location was posterior for 8 of 19 (42%) patients, anterior for 8 (42%) and equatorial for the remaining 3 (16%).

All tumors were of small-medium size with a median apex height value of 3.2 mm (range [2.8–6.5] mm). Typically, tumor base showed an elliptic shape with a median longitudinal diameter of 6.5 mm (range [4.0–11.6] mm) and a median latitudinal diameter of 5.8 mm (range

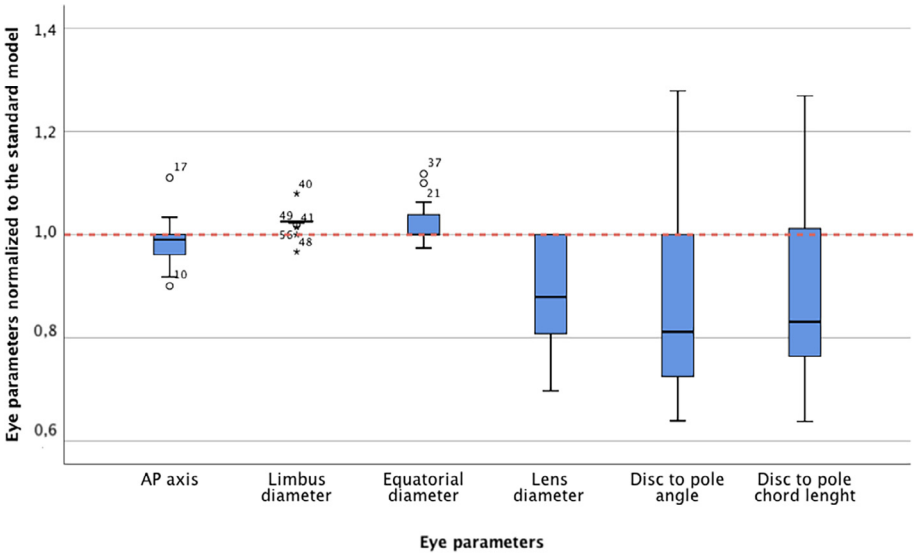

Fig. 3. Computed Tomography (CT)-based eye parameters normalized to the Standard Eye Model (SEM) eye geometry (Antero Posterior axis = 26.2 mm, Equatorial diameter = 24.0 mm, Limbus diameter = 12.0 mm, Lens diameter = 10.0 mm, Disc to pole angle = 21.9 deg, Disc to chord length = 4.2 mm).

[4.0–13.7] mm). Median OD-TC distance was 12.5 [range 5.5–22.2] mm. For all patients, the geometrical reconstruction of the tumor position and dimension was reviewed and validated by an experienced ophthalmologist (M.B.). The ratio of COMS eye parameters obtained by CT to SEM eye geometry ranged from 0.7 to 1.3 (Fig. 3). The SEM model did not accurately describe the real eye geometry, i.e. the CT based model. Lens diameter was always overestimated by the SEM model ($p = 0.002$) and significant discrepancies were observed for the equatorial eye diameter ($p = 0.01$), the AP axis ($p = 0.04$), the limbus diameter ($p = 0.02$), the disc to pole angle ($p = 0.02$) and the disc to pole chord length ($p = 0.02$). The overlap between CT and SEM eye-bulb geometry showed a median Dice coefficient of 0.9 (range [0.8–0.9]) and a median Hausdorff distance of 0.8 mm (range [0.4–1.3] mm).

3.3. Dosimetric evaluation

From the comparison between the D_{mean} values received by the tumor and by eOARs on the whole cohort (Table 2), a statistically significant difference between the two planning strategies was found only for the fovea and the macula ($p = 0.04$). In table 2, the results of the dosimetric comparison performed in patients grouped according to tumor height (≤ 3 mm vs. > 3 mm) was also reported.

In Fig. 4, the tumor and eOAR average DVHs and RDAHs stratified according to tumor position were displayed: tumor coverage was always comparable while, as expected, the doses received by the different eOARs depend on the tumor positions. However, the tumor position also affects the doses estimated by the two different planning schemes. In particular, the adopted planning scheme is critical for the optical structures closest to the tumor as can be observed in the plot reporting the dosimetric results patient by patient (Fig. 5). Indeed, for anterior tumors, differences in D_{mean} values between the SEM-PS and CT–PS schemes can be observed for the lens ($\Delta D_{mean} = 2.9$ Gy [-8.4, 53.0] Gy) and, to less extent, for the retina ($\Delta D_{mean} = 0.4$ Gy [-53.8, 1.6] Gy). On the contrary, for posterior tumors, larger dosimetric discrepancies were observed for the macula ($\Delta D_{mean} = 13.3$ Gy [-9.5, 47.4] Gy) and the fovea ($\Delta D_{mean} = 5.7$ Gy [-9.3, 65.0] Gy).

In Fig. 6, the effect of the planning scheme on macula and optic disc

Table 2
Comparison of the median values of the mean doses (D_{mean}) to the ophthalmic structures at risk (OARs) and to the tumor using Computed Tomography-(CT) Plaque Simulator and Standard Eye Model (SEM) Plaque Simulator planning scheme for all patients and for patients grouped according to tumor height. Prescription dose: 100 Gy to tumor apex.

Structure		All (N = 19) Median (range)			Tumor height					
					≤3 mm (N = 8) Median (range)			> 3 mm (N = 11) Median (range)		
		CT	*SEM*	*p*	*CT*	*SEM*	*p*	*CT*	*SEM*	***p***
OARs D_{mean} (Gy)	Macula	2.8 [0.0–355.0]	4.57 [0.0–351.0]	0.04	22.1 [0.0–320.7]	23.1 [0.0–346.8]	0.03	2.8 [0.0–355.0]	4.6 [0.0–351.0]	0.31
	Optic disc	8.4 [0.0–147.0]	6.7 [0.0–144.0]	0.93	3.3 [0.0–45.3]	5.1 [0.0–56.8]	0.72	8.4 [0.0–147.0]	21.7 [0.0–144.0]	1.00
	Fovea	2.1 [0.0–390.0]	3.1 [0.0–419.6]	0.04	18.7 [0.0–372.0]	21.3 [0.0–419.6]	0.04	2.1 [0.0–390.0]	3.1 [0.0–389.0]	0.48
	Retina	38.8 [3.5–115.0]	36.7 [2.7–114.9]	0.78	36.4 [3.5–115.0]	36.3 [2.7–114.9]	0.33	41.8 [7.8–90.1]	42.3 [7.0–94.1]	0.93
	Lens	5.0 [0.0–211.0]	2.9 [0.0–222.0]	0.32	9.2 [0.0–111.0]	4.9 [0.0–114.0]	0.48	5.0 [0.0–211.2]	2.9 [0.0–222.0]	0.08
Tumor D_{mean} (Gy)	Base	203.4 [164.0–558.0]	202.0 [162.8–537.7]	0.11	175.0 [164.0–537.0]	174.8 [162.8–537.5]	0.75	226.4 [184.0–558.0]	217.0 [187.3–537.7]	0.11
	Volume	160.0 [139.0–324.0]	159.0 [137.7–325.0]	0.85	144.9 [139.0–324.0]	144.9 [137.7–324.5]	0.67	166.0 [149.0–323.0]	162.7 [151.5–325.0]	0.92

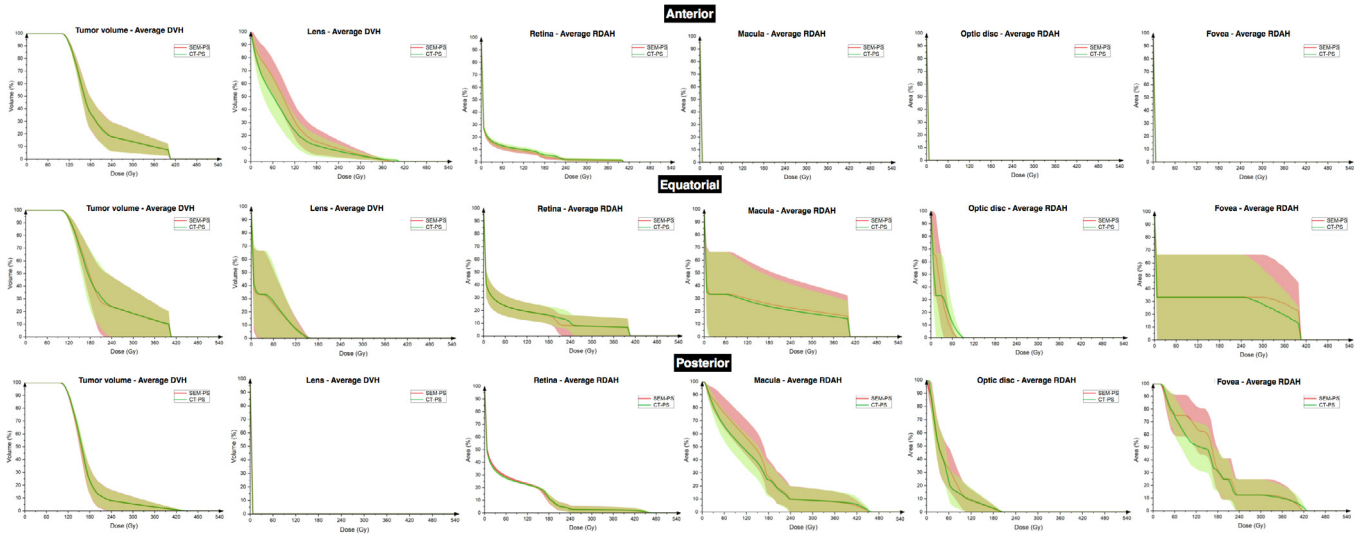

Fig. 4. Comparative average Dose Volume Histograms (DVHs) for tumor volume and lens and Retinal Dose Area Histogram (RDAH) for fovea, macula, retina and optic disc for patients grouped according to tumor position: Computed Tomography (CT) versus Standard Eye Model based Plaque Simulator (PS) planning approaches. The solid spaces indicate the standard error of the mean.

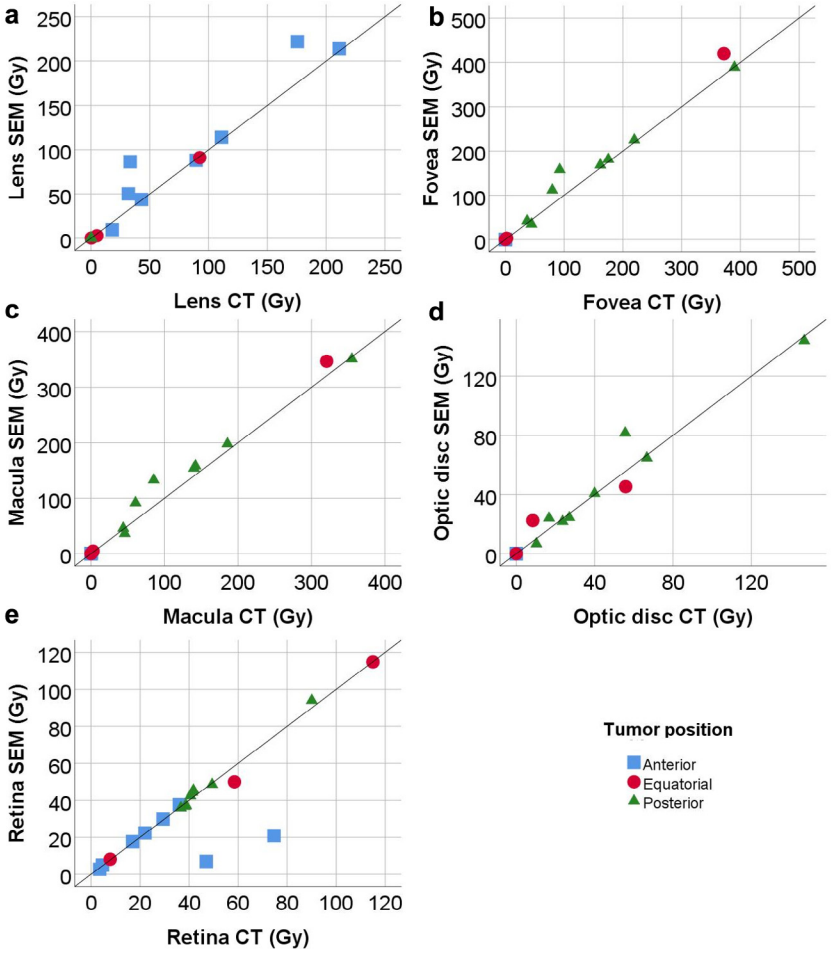

Fig. 5. Individual patients mean doses for ophthalmic structures at risk from Computed Tomography (CT) and Standard Eye Model (SEM) planning approaches. A: anterior tumor position, E: equatorial tumor position, P: posterior tumor position.

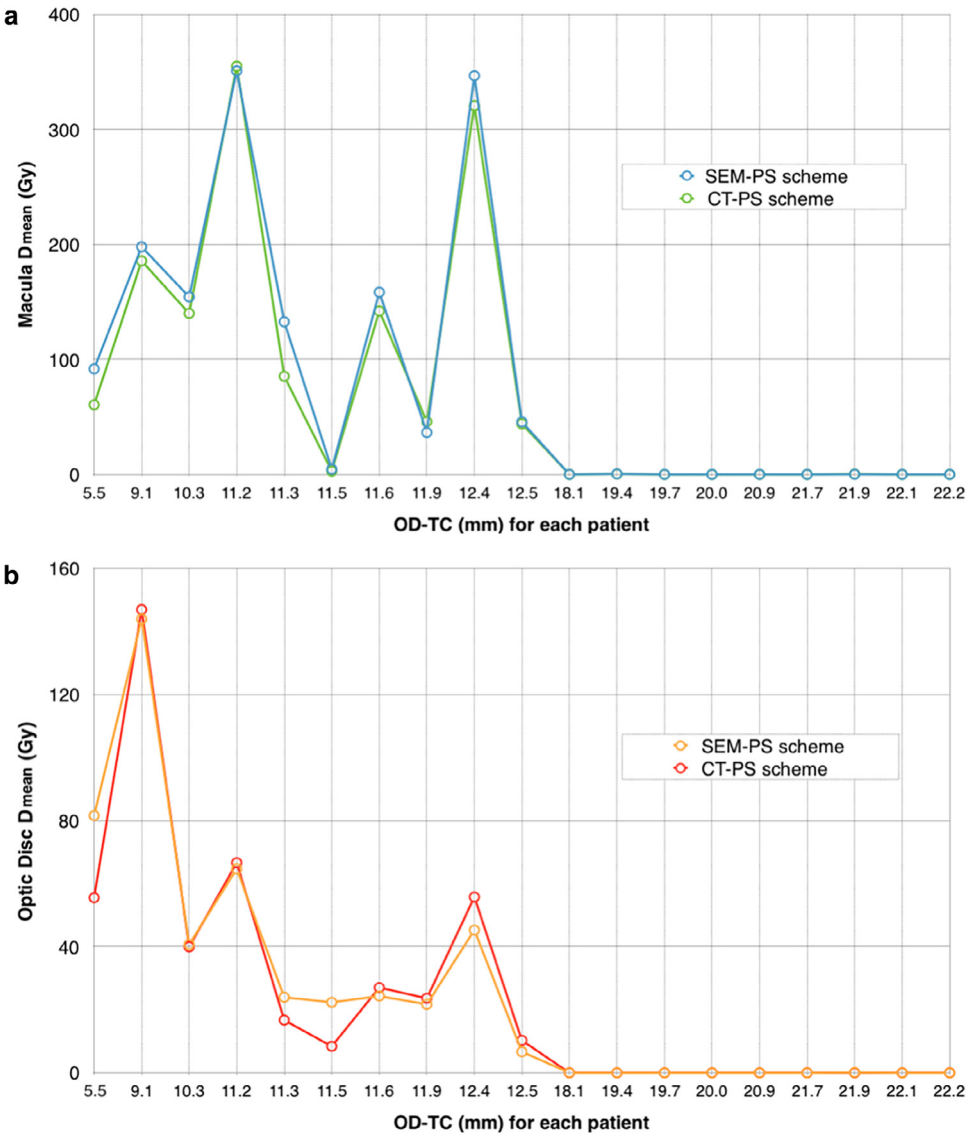

Fig. 6. Mean absorbed doses received by a) macula and b) optic disc for Computed Tomography –Plaque Simulator (CT-PS) and Standard Eye Model –Plaque Simulator (SEM-PS) planning approaches as a function of each patient optic disc - tumor center distance (OD-CT).

D_{mean} values, as a function of the OD-TC distance, was highlighted.

4. Discussion

Brachytherapy with Ru-106 plaques is an effective treatment for ocular melanomas, providing tumor control rate over 90% [27,28]. However, EPB is associated with a range of radiation-induced ocular injuries, which may affect visual outcome and patient quality of life [13]. Diverse clinical and dosimetric variables have been identified as predictors for visual acuity loss in several studies [29]. Those studies, however, reported conflicting results, pointing out the complex mechanisms of visual acuity deterioration following EPB [30].

The radiation induced ocular toxicities include retinopathy, maculopathy, optic neuropathy, neovascular glaucoma, and cataract [29]. Maculopathy and optic neuropathy were reported to be the two most significant complications related to visual loss [13]. The severity of these complications mainly depends on the dose delivered to the respective specific ocular structures and hence an accurate dosimetric evaluation based on personalized treatment planning and on full dose area/volume histograms is required.

The introduction in EPB practice of treatment planning approaches based on 3D imaging would allow for an optimal patient-specific treatment process. Indeed, the use of 3D images, reproducing the real eye geometry, enables to choose the most appropriate plaque and to obtain the optimal tumor coverage to the prescription dose as well as eOARs sparing and toxicity management, by analogy with external beam radiotherapy. However, to the best of our knowledge, a limited number of studies documented the use of CT-based treatment planning in EPB treatments [11,22,31–33], while more commonly a standard SEM eye geometry is applied [7].

With the aim of quantifying the potential advantages of a personalized EPB approach, in this report, we present the workflow for the introduction of CT image-based planning, implemented in PS software for EPB treatments of ocular tumor [26]. A thorough comparison between the dose estimates obtained from treatments planned using a patient specific eye geometry (CT-PS scheme) vs. a standard eye geometry (SEM-PS scheme) was also performed in terms of delivered doses to tumor and eOARs.

As far as the tumor coverage was of concern, for all patients both CT-PS and SEM-PS planning schemes succeeded in obtaining the required dose prescriptions to the tumor base and tumor volume in order to ensure sufficient treatment margins.

However, the 3D reconstruction of the eyeball obtained using the SEM model showed the limits of this approach when compared to the reconstruction obtained using CT images. Significant discrepancies were indeed observed for all the COMS eye parameters. Although, the volume of the eyeball does not show large variations from one individual to another [11], as confirmed by the high Dice coefficient, the value for the Hausdorff distance parameter highlighted a local mismatch due to different patient eye curvatures.

The significant discrepancies in COMS eye parameters between the SEM and CT-based geometry translated into dosimetric discrepancies for the eOARs. In the analyzed cohort, the SEM approach tended to "safely" overestimate the doses to the OARs closest to the tumor (Figs. 4-5). The dosimetric analysis (Table 2) highlighted that the CT-based planning scheme was particularly relevant for the fovea and the macula, for which a significant difference between the two planning approaches can be appreciated. The results of the dosimetric comparison performed in patients grouped according to tumor height showed that the discrepancy between the two planning schemes was particularly significant for small tumors, i.e. with an apical height of 3 mm or less. In particular, for the macula in posteriorly located tumors with height $\leq$ 3 mm, a more pronounced dosimetric discrepancy between the planning schemes was observed (height $\leq$ 3 mm ΔD_{mean} = 14.3 Gy vs. height $>$ 3 mm ΔD_{mean} = 9.3 Gy). An accurate evaluation of the doses received by the fovea and to the macula is critical for the estimation of the risk of radiation retinopathy and maculopathy, respectively. A large recently published retrospective analysis on outcomes after I-125 brachytherapy for posterior uveal melanoma [29] demonstrated indeed that a dose greater than 36 Gy, along with age and tumor apical height, was a risk factor for retinopathy. Total radiation dose delivered to the macula is instead the most important factor related to the development of maculopathy [34].

Similarly, a strong correlation between post-treatment retinal detachment and retina D_{mean} was demonstrated on a cohort of 45 patients receiving Ru-106 plaques brachytherapy [35]. In our analysis, for two patients, with anteriorly located tumors, the mean dose to the retina was dangerously underestimated by the SEM approach (Fig. 5e).

Another common side effects of EPB is radiation-induced optic neuropathy, for which the optic disc-tumor distance parameter was identified as a strong predictor [36]: the OD-TC within one-disc diameter increased the risk of optic neuropathy by a factor of 6. Tien *et al.* [22], reported that a patient-specific eye modeling is recommended, especially for posterior tumor location treated by I-125 brachytherapy and with OD-TC less than 8 mm. In our cohort, only one patient with posterior tumor had an OD-TC less than 8 mm and for that patient the SEM-PS approach did not provide an accurate dose estimation (Fig. 6).

Concerning the doses to the anterior eOARs in patients treated for posterior tumors, the dosimetric advantage of Ru-106 over other isotopes, deriving from its limited range of radiation and its potential vision preservation [37], should be underlined. Our findings on posterior tumor cases, confirmed indeed that the sharp dose fall off of Ru-106 plaques is effective in sparing anterior structures such as the lens (Figs. 4 and 5.a) in agreement with Browne et al. [32] who reported a mean dose to lens of 0.74 Gy (range, 0.0–4.9 Gy) using a Ru-106 plaque. Differently, studies on posterior tumors treated with I-125 plaques reported higher mean doses to lens, e.g. 12.3 Gy [33], 15.2 Gy [31], 12.8 Gy [38].

Remarkably, the dose-complication analysis performed in most of the aforementioned literature was based on eOARs dose parameters extracted from planning based on a standard 3D model of the eye. In the present analysis, we explored instead the introduction in EPB of a CT based treatment planning approach. Overall, our findings are illustrative of the possible under or overestimation of dose delivered to the small or tiny ocular structures and, accordingly, of the related complication risk when a standard eye geometry is applied. This highlights the value for a personalized dosimetry if robust studies on the development of normal tissue complication probability models [39] have to be undertaken for an adequate understanding of visual acuity deterioration and late complications in EPB treatments.

In this framework, an additional issue to take into account is the effect of dose uncertainties on the estimated eOARs doses, particularly for those structures where the dose levels are close to their tolerance values. Improvements in dose calculation accuracy within the eye by the use of model-based dose calculations might result in more accurate correlation between doses to critical structures and complication rates. Indeed, doses to eye tissues may differ markedly from those calculated when accounting for the actual eye tissues, up to 27% [12].

Our analysis represents a proof-of-concept study on the introduction of a CT based dosimetry in EPB clinical routine. More CT data is required and further research and larger studies are warranted, in particular to further clarify the effects of patients' stratification according to the different tumor position (i.e. anterior, equatorial, posterior) and tumor dimension. In addition, it should be underlined that in the current study we only examined a single plaque source with a fixed diameter of 20 mm. The reduction of plaque size has been reported to decrease the D_{mean} to lens, optic nerve and macula by more than 60% [14] while Miguel et al. [29] found the size of the plaque ($>$ 16 mm) to be an important risk factor for retinal detachment. A reduction of plaque size represents an important factor that should be considered for further optimizing EPB treatments.

5. Conclusion

Our work explores the dosimetric effect of personalized CT-based planning with PS software in EPB treatment. The obtained findings showed the robustness of the framework and illustrated the importance for a personalized treatment planning, paving the way for future toxicity studies. The dosimetric accuracy achievable with CT-PS EPB treatment planning may be useful to identify those patients who could benefit the most from a personalized eye dosimetry in EPB with the aim of ensuring the optimal treatment outcome in terms of tumor coverage and eOARs sparing.

Funding

This research did not receive any specific grant from funding agencies in the public, commercial, or not-for-profit sectors.

Acknowledgement

We want to thank Prof. M. Astrahan for providing us Plaque Simulator software license for research purpose.

References

[1] Virgili G, Gatta G, Ciccolallo L, Capocaccia R, Biggeri A, Crocetti E, et al. Incidence of uveal melanoma in Europe. Ophthalmology 2007;114:2309–15.
[2] Grange JD, Gérard JP, Kodjikian L, Rouberol F, Duquesne N, Romestaing P, et al. Quinze ans d'expérience dans le traitement des mélanomes de l'uvée postérieure par la radiothérapie. Cancer/Radiothérapie 1999;3:89s–97s.
[3] Diener-West M, Earle JD, Fine SL, Hawkins BS, Moy CS, Reynolds SM, et al. The COMS randomized trial of iodine 125 brachytherapy for choroidal melanoma, III: initial mortality findings. COMS Report No. 18. Arch Ophthalmol 2001;119:969–82.
[4] Nag S, Quivey JM, Earle JD, Followill D, Fontanesi J, Finger PT. The American Brachytherapy Society recommendations for brachytherapy of uveal melanomas. Int J Radiat Oncol Biol Phys 2003;56:544–55.
[5] Brualla L, Zaragoza FJ, Sauerwein W. Monte Carlo simulation of the treatment of eye tumors with 106-Ru plaques: a study on maximum tumor height and eccentric placement. Ocular Oncol Pathol 2015;1:2–12.
[6] Naseripour M, Jaberi R, Sedaghat A, Azma Z, Nojomi M, Falavarjani KG, et al. Ruthenium-106 brachytherapy for thick uveal melanoma: reappraisal of apex and base dose radiation and dose rate. J Contemp Brachytherapy 2016;8:66–73.
[7] Stockel E, Eichmann M, Fluhs D, Sommer H, Biewald E, Bornfeld N, et al. Dose distributions and treatment margins in ocular brachytherapy with 106Ru eye plaques. Ocul Oncol Pathol 2018;4:122–8.
[8] Tagliaferri L, Pagliara MM, Boldrini L, Caputo CG, Azario L, Campitelli M, et al. INTERACTS (INTErventional Radiotherapy ACtive Teaching School) guidelines for quality assurance in choroidal melanoma interventional radiotherapy

(brachytherapy) procedures. J Contemp Brachytherapy 2017;9:287–95.
[9] Busoni S, Fedeli L, Belli G, Genovese E, Cannatà V, Gori C, et al. Pre and post operative radiation protection in Ru-106 brachytherapy ophthalmic plaque surgery and related material shielding properties. Physica Med 2019;57:245–50.
[10] Gerbaulet A. The GEC ESTRO handbook of brachytherapy; 2002.
[11] Brualla L, Sempau J, Zaragoza FJ, Wittig A, Sauerwein W. Accurate estimation of dose distributions inside an eye irradiated with 106Ru plaques. Strahlenther Onkol 2013;189:68–73.
[12] Morrison H, Menon G, Larocque MP, van Veelen B, Niatsetski Y, Weis E, et al. Advanced Collapsed cone Engine dose calculations in tissue media for COMS eye plaques loaded with I-125 seeds. Med Phys 2018;45:3349–60.
[13] Tseng VL. Complications from plaque versus proton beam therapy for choroidal melanoma: a qualitative systematic review. J Cancer Therapy 2016;7:169–85.
[14] Heilemann G, Fetty L, Dulovits M, Blaickner M, Nesvacil N, Georg D, et al. Treatment plan optimization and robustness of (106)Ru eye plaque brachytherapy using a novel software tool. Radiother Oncol 2017;123:119–24.
[15] Zaragoza FJ, Eichmann M, Fluhs D, Wittig A, Sauerwein W, Brualla L. Monte Carlo simulation of the treatment of uveal melanoma using measured heterogeneous (106)Ru plaques. Ocul Oncol Pathol 2019;5:276–83.
[16] Mostafa L, Rachid K, Ahmed SM. Comparison between beta radiation dose distribution due to LDR and HDR ocular brachytherapy applicators using GATE Monte Carlo platform. Physica Med 2016;32:1007–18.
[17] Astrahan MA, Luxton G, Jozsef G, Kampp TD, Liggett PE, Sapozink MD, et al. An interactive treatment planning system for ophthalmic plaque radiotherapy. Int J Radiat Oncol Biol Phys 1990;18:679–87.
[18] Thomson RM, Furutani KM, Kaulich TW, Mourtada F, Rivard MJ, Soares CG, et al. AAPM recommendations on medical physics practices for ocular plaque brachytherapy: report of task group 221. Med Phys 2020;47(5):e92–124.
[19] The COMS. randomized trial of iodine 125 brachytherapy for choroidal melanoma: V. Twelve-year mortality rates and prognostic factors: COMS report. No 28 Arch Ophthalmol 2006;124:1684–93.
[20] Astrahan MA. A patch source model for treatment planning of ruthenium ophthalmic applicators. Med Phys 2003;30:1219–28.
[21] Berger MJ. Distribution of absorbed dose around point sources of electrons and beta particles in water and other media. J Nucl Med 1971;Suppl 5:-23.
[22] Tien CJ, Astrahan MA, Kim JM, Materin M, Chen Z, Nath R, et al. Incorporating patient-specific CT-based ophthalmic anatomy in modeling iodine-125 eye plaque brachytherapy dose distributions. Brachytherapy 2017;16:1057–64.
[23] Dice LR. Measures of the amount of ecologic association between species. Ecology 1945;26:297–302.
[24] Huttenlocher DP, Klanderman GA, Rucklidge WA. Comparing images using the hausdorff distance. IEEE Trans Pattern Anal Mach Intell 1993;15:850–63.
[25] Taha AA, Hanbury A. Metrics for evaluating 3D medical image segmentation: analysis, selection, and tool. BMC Med Imaging 2015;15:29.
[26] Astrahan MA. The retina dose-area histogram: a metric for quantitatively comparing rival eye plaque treatment options. J Contemp Brachytherapy 2013;5:23–32.
[27] Seregard S. Long-term survival after ruthenium plaque radiotherapy for uveal melanoma. A meta-analysis of studies including 1,066 patients. Acta Ophthalmol Scand 1999;77:414–7.
[28] Espensen CA, Appelt AL, Fog LS, Thariat J, Gothelf AB, Aznar MC, et al. Tumour control probability after Ruthenium-106 brachytherapy for choroidal melanomas. Acta Oncol 2020;1–8.
[29] Miguel D, de Frutos-Baraja JM, López-Lara F, Saornil MA, García-Álvarez C, Alonso P, et al. Radiobiological doses, tumor, and treatment features influence on outcomes after episcleral brachytherapy. A 20-year retrospective analysis from a single-institution: part II. J Contemp Brachytherapy 2018;10:347–59.
[30] Espensen CA, Appelt AL, Fog LS, Gothelf AB, Thariat J, Kiilgaard JF. Predicting visual acuity deterioration and radiation-induced toxicities after brachytherapy. Cancers 2019;11.
[31] Berry JL, Dandapani SV, Stevanovic M, Lee TC, Astrahan M, Murphree AL, et al. Outcomes of choroidal melanomas treated with eye physics: a 20-year review. JAMA Ophthalmol 2013;131:1435–42.
[32] Browne AW, Dandapani SV, Jennelle R, Stevanovic M, Lee TC, Murphree AL, et al. Outcomes of medium choroidal melanomas treated with ruthenium brachytherapy guided by three-dimensional pretreatment modeling. Brachytherapy 2015;14:718–25.
[33] Le BHA, Kim JW, Deng H, Rayess N, Jennelle RL, Zhou SY, et al. Outcomes of choroidal melanomas treated with eye physics plaques: a 25-year review. Brachytherapy 2018;17:981–9.
[34] Singh AD, Pabon S, Aronow ME. Management of radiation maculopathy. Ophthalmic Res 2012;48(Suppl 1):26–31.
[35] Heilemann G, Fetty L, Blaickner M, Nesvacil N, Zehetmayer M, Georg D, et al. Retina dose as a predictor for visual acuity loss in (106)Ru eye plaque brachytherapy of uveal melanomas. Radiother Oncol 2018;127:379–84.
[36] Summanen P, Immonen I, Kivela T, Tommila P, Heikkonen J, Tarkkanen A. Radiation related complications after ruthenium plaque radiotherapy of uveal melanoma. Br J Ophthalmol 1996;80:732–9.
[37] Pe'er J. Ruthenium-106 brachytherapy. Dev Ophthalmol 2012;49:27–40.
[38] Krema H, Heydarian M, Beiki-Ardakani A, Weisbrod D, Xu W, Laperriere NJ, et al. Dosimetric and late radiation toxicity comparison between iodine-125 brachytherapy and stereotactic radiation therapy for juxtapapillary choroidal melanoma. Int J Radiat Oncol Biol Phys 2013;86:510–5.
[39] Palma G, Monti S, Conson M, Pacelli R, Cella L. Normal tissue complication probability (NTCP) models for modern radiation therapy. Semin Oncol 2019;46:210–8.